Finite element analyses of mode I interlaminar delamination in z-fibre reinforced composite laminates

Marcello Grassi & Xiang Zhang[*]

Aerospace Engineering Group, School of Engineering, Cranfield University, Bedford, MK43 0AL, UK

Abstract. This paper presents a detailed numerical study of the mode I interlaminar fracture of carbon/epoxy composite laminates with z-fibre reinforcement. The study was performed using a double cantilever beam configuration. A finite element model was developed using thick-layered shell elements to model the composite laminates and non-linear interface elements to simulate the through thickness reinforcements. An existing micro-mechanical solution was employed to model the material behaviour of the interface element. The numerical analysis showed that z-fibre pinning were effective in bridging delamination when damage had propagated into the z-fibre field; these pins provided crack closure forces that shielded the delamination crack from the full delaminating force and moment due to applied loads. Therefore, the z-fibre technique significantly improves the crack growth resistance and hence arrests or delays delamination extension. The numerical results were validated against experimental data. With reference to structural integrity this technique can be used to design a more damage tolerant structure.

Nomenclature

d	z-fibre embedding depth	d_z/r_z	z-fibre diameter/radius
da	incremental crack growth length	l_s	z-fibre slip length
A_t	z-fibre cross-section area	B	width of DCB specimen
D	length of large scale bridging area	$F(u)$	load-displacement function of a z-fibre
G_I	strain energy release rate in mode I fracture	G_{IC}	delamination toughness of a laminate
W	total external work	U_e	stored elastic strain energy
U_k	kinetic energy	U_{ir}	irreversible energy dissipation
Γ	energy for newly created fracture surface	Φ_{ir}	energy dissipation rate
ψ_z	discrete bridging load for a single z-fibre	ϕ	z-fibre insertion angle
Φ_z	distributed bridging loads for a group of z-fibres		
τ	frictional stress between z-fibre and laminate during a z-fibre pullout		

1. Introduction

Delamination is the most detrimental failure mode in aerospace composite structures. To improve structural damage tolerance, new composites with through-thickness reinforcements (TTR) such as z-fibre pinning (or z-pinning), stitching, and 3D woven fabrics have been developed and they are often referred to as 3D reinforced laminates [1-4]. Several experimental investigations have shown that these new composites offer significant improvements in fracture toughness, impact resistance, compression-after-impact strength, interlaminar strength, and the stiffener's pull-off strength [5-12]. However, the in-plane properties of the TTR composites suffer some degree of reduction [13-15].

When a delamination crack develops, TTR forms a bridging area at the crack wake that shields the delamination crack from the interlaminar stresses. The TTR bridging mechanics will modify the crack-tip strain energy release rate and hence reduce the crack propagation rate. When the fibre bridging length (the length of the crack where bridging occurs) is restricted to a zone that is much smaller in length than any specimen dimensions (small scale bridging), the rising crack growth resistance (R-curve) can be regarded

---

[*] Corresponding author. Tel.: +44 1234 754621; Fax: +44 1234 758203.
E-mail address: xiang.zhang@cranfield.ac.uk (X. Zhang)

as a material property. However, for many crack growth problems the bridging length can be comparable with or exceed the specimen dimension. This is called large-scale bridging (LSB). In situations of LSB the delamination process cannot be correctly described by the linear elastic fracture mechanics (LEFM) theory because the order of the magnitudes of the bridging zone length and the total crack length become comparable, and the delamination behaviour is not solely controlled by a single parameter, such as the fracture toughness of the material [16-21]. The R-curve is no longer a material property; it also depends on the specimen geometry [17]. A robust tool is required for the analysis.

This paper deals with z-fibre reinforced carbon/epoxy composite, which is defined as laminate with up to 5% volume fraction of fibrous or metallic reinforcement in the thickness direction. Previous studies have shown that z-pinning effect on stress singularity zones, such as crack-tip or laminate free edges where delamination normally starts, is very small if z-fibres are still in the intact part of the laminate [13, 22]. Therefore the key task is to quantify z-pinning effect on delamination propagation rather than initiation. The mode I interlaminar fracture has been a topic for many researchers using the double cantilever beam (DCB) configuration [19-21]. Analytical models solve the constitutive and equilibrium equations of the DCB by using the simple or shear deformation beam theories combined with discrete [19] or linear continuous bridging loads [20-21] for the z-fibre simulation. Under certain assumptions closed-form solutions were derived outlining the large scale bridging mechanisms and their effects on the strain energy release rate (G_I) of the laminate. In these beam models boundary conditions applied at the crack tip usually underestimate the G_I values at the crack front. Besides, when the bridging tractions are expressed as functions of the crack displacement, even using linear functions the resulting crack behaviour is generally nonlinear [21]. Moreover the DCB arms of a z-pinned specimen usually subject to large crack opening displacements due to large increments of the applied load required propagating the delamination; this will introduce additional nonlinear behaviour.

Another challenging problem facing the modellers is the simulation of the z-fibre behaviour. Research has shown the mechanisms of z-fibres bridging a delamination crack [5, 23]. The failure process often involves z-fibre debonding and sliding out from the laminate. From the modelling point of view, those complex damage mechanisms can be incorporated into a bridging function $F(u)$, that is the relation between the bridging traction force vector (F) acting on the fracture surfaces and the displacement vector of the z-fibre cross section at delamination wake (u)[24]. Depending on the fracture mode ratio and the kind of TTR, i.e. stitching or z-pining, several micro-mechanical models have been developed for a single bridging entity [25-28]. These bridging functions may be implemented into a structural model.

The advancement of the finite element methods has provided a robust and flexible tool to solve the aforementioned nonlinear problems [29-33] and to calculate accurately the G_I values and mode ratios at the crack front [34-38]. For example, a global-local FE analysis used 3D FE models with either layered shell or solid brick elements in the fracture critical zones with the boundary conditions obtained from the global analysis [38]. It has the capability to study in details the damage development in the key areas and optimise the computational effort [39]. Another work employed 2D plane-strain FE analysis to study a z-pinned DCB by inserting an experimentally derived bridging law to find the effect of various z-fibre properties [23]. A strong dependence on the availability of experimental data was noticed; hence different tests would be required for different material and z-pin quality.

This paper presents a detailed 3D FE model for studying the characteristics of delamination fracture with z-fibre effect. The work is aimed at the mode I model that can be further developed to model other single or mixed failure modes providing that the correct boundary conditions and micro-mechanical solutions are implemented. The objective is to develop a design approach that combines the finite element method with an existing micro-mechanical material model so that the effect of z-pinning on delamination propagation may be predicted. Following problems have been investigated: effect of z-fibres on delamination growth

and arrestment, the LSB effect, stress field in z-pinned laminate during delamination growth, influence of z-pin properties and densities, and the energy balance associated with fracture process. The numerical solutions were validated against available experimental data [7, 8].

2. Problem Statement

2.1. Theoretical beam model for large scale bridging.

The double cantilever beam (DCB) configuration illustrated in Fig 1a is often used to study the mode I delamination problem. From the modelling point of view each DCB arm can be treated as an elastic beam subjected to a distributed or discrete traction force $\Phi_z(x)$ simulating the bridging action of the z-pins as shown schematically in Fig. 1b. The Euler-Bernoulli differential equations in the bridging domain and beyond are:

$$EI\frac{d^4\delta}{dx^4}+\Phi_Z(x)=0 \quad (0<x\leq D) \qquad (1)$$

$$EI\frac{d^4\delta}{dx^4}=0 \qquad (D<x) \qquad (2)$$

Where, δ denotes the transverse deflection of the beam, D the length of the LSB zone, EI the flexural rigidity of the beam, and $\Phi_z(x)$ the bridging forces.

The data given in the problem, i.e. EI, Φ_z, are not continuous in the entire domain. However, there have been attempts to solve the above equations analytically. Mabson and Deobald [20] assumed a linear relationship for single z-fibre traction force and displacement and a linear distribution for $\Phi_z(x)$. A closed-form solution was derived and useful design curves were obtained for two forms of through-thickness reinforcements, i.e. stitching and z-pinning. Liu and Mai [19] solved Eq. (1) by assuming a series of discrete non-linear bridging forces and using an approximate iterative method to obtain the solution. Both papers used the Euler-Bernoulli beam theory and analytically derived bridging load-displacement relationship for the z-fibre traction force simulation. Massabo and Cox developed another closed-form solution under the crack-tip shear deformation assumption using different linear bridging laws, i.e. constant, proportional linear, and general linear [21].

In fact, the so-called large-scale bridging traction loads acting over the active bridging zone (D in Fig.1b) depends on many variables, so it may be described more generically as a complex function $\Phi_z(x)$:

$$\Phi_Z(x)=\Phi_Z(\psi_Z,c,D,P,u,EI) \qquad (3)$$

where, c is the z-fibre density, D the length of bridging zone involving many rows of z-pins, P the applied load, u the displacement vector within the LSB area, EI the flexural rigidity of the laminate, and ψ_Z the bridging load (force or moment) of a single i[th] z-fibre that itself is a function of many parameters depending on the micro-mechanical model used:

$$\psi_Z=\psi_Z(u,\theta,\phi,\tau,\tau_0,\sigma_0,E_z,r_z,A_t,d) \qquad (4)$$

where, u is the displacement vector of the z-fibre cross section at delamination wake (Fig. 2), θ z-pin rotation in the x-z plane, ϕ z-fibre insertion angle, τ frictional shear stress at the z-fibre and laminate interface during frictional sliding, τ_0 shear flow stress due to sliding displacement (u_1), σ_0 the axial stress of the z-pin rod, E_z the Young's modulus of z-fibre, r_z z-fibre radius, A_t cross sectional area of z-pin, and d z-fibre insertion depth into the laminate.

In this study, the bridging effect is modelled by implementing the discrete bridging forces, Eq. (4), into a finite element model.

2.2 *Energy balance during large scale bridging.*

The ability of a composite structure to absorb the energy reduces the damage development. Therefore for design purpose it is important to know the energy absorption capability of a z-pinned laminate during delamination growth. According to the Griffith fracture energy theory [40], an elastic body subjected to externally applied loads must satisfy the following energy balance:

$$W = U_e + U_k + U_{ir} + \Gamma \tag{5}$$

where, W is the external work, U_e the stored elastic energy, U_k the kinetic energy, U_{ir} the dissipated energy due to some irreversible mechanisms, Γ the energy dissipation during the formation of a new crack surface, therefore it is consumed only in a very small cohesive zone at the crack front. An increment in the crack area (dA) will require energy increment, but the overall energy balance of the system expressed by Eq. 5 remains valid:

$$dW = dU_e + dU_k + dU_{ir} + d\Gamma \tag{6}$$

For static fracture tests, the typical experimental loading rates are around 1 mm/min under a displacement-controlled condition so the variation of the kinetic energy of the system is negligible. If the crack is assumed to be self-similar and $dA=B\cdot da$, then the available elastic energy in the system per unit crack area can be expressed as:

$$\frac{1}{B} \cdot \left(\frac{dW}{da} - \frac{dU_e}{da} \right) = \frac{1}{B} \cdot \left(\frac{d\Gamma}{da} + \frac{dU_{ir}}{da} \right) \tag{7}$$

With reference to mode I delamination of the z-pinned laminate, define:

$$G_I = \frac{1}{B} \cdot \left(\frac{dW}{da} - \frac{dU_e}{da} \right), \ G_{IC} = \frac{1}{B} \frac{d\Gamma}{da}, \ \Phi_{ir} = \frac{1}{B} \cdot \frac{dU_{ir}}{da} \tag{8}$$

Where, G_I is the strain energy release rate due to applied force, G_{IC} the intrinsic delamination toughness of the laminate, and Φ_{ir} the energy dissipation rate due to the irreversible z-pin pullout process, which is the toughening mechanism of z-pinned laminates in terms of the fracture energy theory.

Therefore, the Griffith fracture criterion for z-pinned laminates can be written as:

$$G_I = G_{IC} + \Phi_{ir} \tag{9}$$

Here the strain energy release rate G_I equals to the toughness of the z-pinned laminate during crack growth, which is the crack growth resistance.

Z-pinned laminates should be designed to achieve high value of U_{ir} that under certain crack conditions may exceed the energy necessary for the creation of a new fracture surface, hence to increase the fracture toughness. Thus the magnitude of U_{ir} is among the parameters that must be determined for the characterization of the fracture behaviour of z-pinned laminates. The LEFM theory assumes that all energy dissipations for the creation of a new fracture surface dA are included in the Γ term. It is hence postulated that during interlaminar delamination in a conventional un-reinforced laminate the order of magnitude of other energy dissipation occurring away from the damage front zone are negligible, i.e. $U_{ir} = 0$. The novel and strong point dealing with through-thickness reinforced laminates is the large amount of energy absorption associated with the large scale bridging mechanics; hence the appearance of the U_{ir} and Φ_{ir} terms in the above derived equations.

3. Modelling procedures

3.1 Model for z-fibre bridging mechanics

The micro-mechanical model developed by Cox [27] is used in this study. It is capable of dealing with mixed mode loading and inclined through-thickness reinforcements. The essential mechanisms of angled z-fibres bridging a delamination crack [5] are summarized in the following:

Z-fibre debonding from laminate, frictional sliding and pulling out from the laminate;
Development of axial tension in the z-fibre rod during pullout process;
Axial shear deformation with matrix damage and splitting cracks in the interior of the z-fibre;
Ploughing of the z-fibre rod laterally through the laminate, which resists lateral displacements via matrix deformations and micro-cracking.

The output of the micro-mechanical model is a relationship between the bridging tractions applied to the fracture surfaces by the z-fibre and the crack opening and sliding displacements. For a single z-pin a traction vector (F) is introduced along with the total crack displacement vector (u), which has two components being defined in the local reference frame. This bridging traction law $F(u)$ can incorporate all those aforementioned complex phenomena. The simulation of the different mechanisms by $F(u)$ also depends on the initial orientation of the z-pins (ϕ) and the applied mode ratio. Under the mode I loading condition and when z-fibres are inserted at right angles (90°) to the principal in-plane axes ($\phi = 0^{\circ}$ in Cox' original model), the geometric parameters and boundary conditions chosen for this study are illustrated in Fig. 2. It is assumed that the sliding displacement (u_1) and the in-plane z-pin rotation (θ) due to the plastic shear deformation within the pin, were negligible and therefore the plastic shear flow $\tau_0 = 0$ and the compressive transverse stress in the rod $\sigma_n = 0$.

The z-fibre debonding and pullout resisted by friction is the dominant bridging mechanics, therefore in this study the micro-mechanical model of Eq. (4) is described by the Cox' bridging function, i.e. $\psi_z = F(u)$, which is a mono-dimensional function that relates the opening displacement ($u = u_3$) to the force exerted along the z direction in the crack reference frame. Fig. 2 shows the slip length (l_s) has already attained the z-fibre embedded depth (d) and the pullout process is already propagated with a displacement s.

A set of computed force vs. deflection ($F–u$) curves are plotted in Fig. 3. The range of the friction stress for fibre pullout was assumed to be between 10-80 MPa [23, 25]. Fig. 3 shows that there are two main mechanisms, i.e. z-fibre slips through the laminate developing axial tension due to the elastic stretching (Fig. 3a) and when the slip zone reaches the end of the bridging rod ($l_s = d$), z-fibre slides and pulls out of the laminate as a rigid body (Fig. 3b). It is clear that in this specific z-fibre configuration, the amount of energy dissipated during the frictional sliding stage is much higher than the energy absorbed by the z-fibre slip stage. In the micro-mechanical model developed by Zhang et al [26], the same failure process was modelled but the elastic stretching of the fully bonded z-fibre and debonding propagation was also considered. The energy absorbed during these phases was only a small percentage (1-2%) of the total energy absorbed by the pullout failure process. It is then suggested that the assumption of the z-fibre being already debonded would only introduce a small error in the FE simulation.

To implement the above micro-mechanical solution into an FE model, z-pins in the delamination wake were modelled by the interface element, *COMBIN39,* available from the *ANSYS* element library [33]. This is a 1D element with the capability of taking generalized non-linear force-deflection relations. The option provides a uniaxial tension-compression element with up to three degrees of freedom at each node, i.e. translations in the *x, y*, and *z* directions; no bending or torsion was considered. The element is defined by two initially coincident nodes. When the delamination propagated a generalized force-deflection curve $F(u),$ which is defined in a local reference frame, was adopted.

3.2 DCB finite element model

An FE model was created for a z-pinned DCB specimen (Fig. 4a) as shown in Fig. 4b. The numerical model consists of two different mesh zones: a coarse mesh for the undamaged part and a fine mesh in the delamination growth zone. The area where interlaminar delamination was expected to grow was modelled with two sub-laminates having the nodes coupled with an offset position at the delamination interface. The displacement matrices of the upper and lower sub-laminate were simplified by the coupled field assumption. The positioning of the z-fibre elements at the interface is also indicated in Fig. 4b. The distance between two consecutive interface elements depends on the assumed z-fibre density and diameter. Table 1 shows some standard z-pin diameters and densities that were studied here. The non-linear layered shell element (Shell-91) from the ANSYS element library was found suitable to model the composite laminate. It has several useful properties such as shape functions with transverse shear deformations [35], large deformation capability, quadratic element formulation [36], defining laminate stacking sequences and nodal offset positions through the thickness [38]. Cylindrical bending boundary conditions were imposed; whilst the clamped beam end is to avoid numerical errors for an insufficiently constrained model. The multiple-point constraint equations were applied to the nodes placed at the free ends to impose equally applied displacement.

Table 1. Distances between two adjacent z-fibres for typical z-fibre arrays. (Unit mm)

Z-fibre density	0.5%	1%	2%	4%
Z-fibre diameter				
0.28	3.51	2.48	1.75	1.24
0.50	6.39	4.52	3.20	2.26

Based on the fracture criterion defined by Eq. (9), the FE analysis allows a delamination crack to propagate when:

$$G_I - \Phi_{ir} \geq G_{IC} \qquad\qquad (10)$$

where, $(G_I - \Phi_{ir})$ is the net energy release rate at the crack tip considering the z-pin traction forces, which if larger than G_{IC} will cause equilibrium crack growth to occur.

The value $(G_I - \Phi_{ir})$ was calculated using the virtual crack closure technique (VCCT) [21] with the advantage of only a single FE run being required. The nodal forces and displacements at delamination front needed for the calculation were computed in a local reference frame following the crack propagation. Using the ANSYS programmable language, several subroutines were developed and implemented into the main code to model the following features: z-fibre material model, auto-meshing, computation of $(G_I - \Phi_{ir})$ values, non-linear iterative solutions, and delamination growth simulation.

In order to simulate the experimental work in [8], a displacement-controlled non-linear FE analysis was performed using the full Newton-Raphson method in order to reduce the numerical error. A standard force and moment convergence criterion was used for the Newton-Raphson method and several other parameters were also controlled and defined in order to optimise the iterative numerical solution, computational time and accuracy [33]. The solution-algorithm performs two main tasks: (1) if the criterion described by Eq. (10) is not met then the applied displacement is increased by a value of δ_i and the $(G_I - \Phi_{ir})$ value at the crack-front are re-computed; (2) if the failure criteria is satisfied then the nodes at the delamination front are uncoupled, the applied displacement remains unchanged, and a new calculation iteration is performed. The structural stiffness matrix [K] is updated for every new crack position. During the solution process the procedure also checks for bending failure of the beam and the analysis will be terminated at the maximum delamination length of 30 mm. Convergence tests were undertaken with different mesh densities at the crack front and different applied incremental displacement. In this study, numerical convergence was

achieved by using the mesh size of 0.5 mm for the delamination growth front and incremental displacement of 0.2 mm.

4. Results & Discussion

4.1 Numerical examples

The geometrical parameters for the DCB specimen modelled in this work (Fig. 4a) were taken from the experimental tests in [23]. The DCB length (*L*) and width (*B*) are 160 and 20 mm, respectively, and the range of the laminate thickness (*2t*) is between 3 and 6 mm. The length of the initial crack (*a_o*) is 50 mm. The distance between the initial crack tip and the first z-pin row is 5 mm, and the total length of the pinned area is 25mm (Fig. 4a). The DCB is made of carbon-epoxy IMS/924 unidirectional plies with a single ply thickness of 0.125 mm and the following typical elastic properties: $E_{11}=138$ *GPa*, $E_{22}=11GPa$, $G_{12}=4.4GPa$, $v_{12}=0.34$. The z-fibres are made of carbon fibres. Four different z-fibre volume densities (0.5%, 1%, 2%, & 4%) and two typical z-fibre diameters (0.28 and 0.51 mm) were simulated. In order to take account of the z-pinning effect on the laminate elastic properties the elastic bending stiffness in the z-pinned area was modified according to a previous work[13]. Different z-fibre insertion depths (*d*) were also studied to cover the range of partially and fully pinned laminates. Un-reinforced laminates were also modelled as the control cases.

4.2 Z-fibre effects on delamination propagation

The force-displacement curve is a good indication of the fracture process of a DCB specimen. At the first load step an applied displacement of 4 mm will bring the model close to the fracture condition described by Eq. (10). An incrementally applied displacement of 0.1 mm ($\delta/2$) for each DCB arm is then applied. Firstly, the control case of an unpinned DCB specimen is shown in Fig. 5. The linear rising part of the curve refers to the elastic deformation of the DCB arms without any damage propagation (first load step). When the fracture criterion (Eq. 10) was satisfied, delamination started to propagate. This initial crack extension occurred at the load level of 40 N. This load level is a turning point from which the external load decreased with the increasing applied displacement. The experimentally measured data are also shown in the same figure, and the agreement is excellent. The control specimen analysis was also useful to calibrate the G_{IC} value in Eq. (10). For this case the value of 250 J/m^2 was used for G_{IC}, which was also used as the critical value for the z-pinned laminates at the crack-tip zone.

Fig. 6 shows the load-displacement curves of a z-pinned DCB configuration with an area density of 0.5%. The z-fibres had a diameter of 0.28 mm. The critical load for initial delamination propagation was almost the same as the un-reinforced laminate, around 40 N as indicated by the first load drop. However, the force quickly picked up and the curve shape after the initial delamination growth altered completely, i.e. from a declining P-δ curve of unpinned case (Fig. 5) to a rising curve (Fig. 6). This is because delamination has propagated into the z-fibre field where the resistance to damage growth is significantly higher than that of the unpinned case. The sudden drop of the load at about 40N was due to the initial delamination propagation within the first 5 mm zone where no z-fibres were placed (Fig. 4a). After passing the first z-fibre row, the bridging mechanics worked by rising the external load (*P*) necessary to propagate the damage further. Then at the load of 48 N there was another drop in the external load. This corresponds to another damage growth just before meeting the next row of z-fibres. This phenomenon repeated regularly exhibiting stable crack propagation behaviour. This distinct shape of the P-δ curves in a through-thickness reinforced laminate was referred as the "stick-slip" behaviour in the literature [9,11]; it was assumed to be caused by the presence of z-fibre or stitching rows at regular intervals. For a lower z-fibre density, a direct relation between the number of working z-fibre rows and the observed local load drops of the P-δ curve could be established. In this case (Fig. 6), five z-fibre rows were actively involved in the bridging field.

According to the experimental work in [23], a suitable constant value of the frictional stress of 15 MPa was implemented in the interface elements.

Fig. 7 shows a higher density (2%) pinning case, in which two DCB specimens reinforced with 0.28 mm diameter z-fibres were simulated. Both the numerical simulation and experimental data are shown in the same graph for comparison. Firstly, the "stick-slip" characteristic in the P-δ curves of Fig. 6 (lower pin density of 0.5%) seemed to have disappeared in Fig. 7. This is because that more z-pins were in the bridging zone for the high-density case. The P-δ curves also show a maximum load value of about 180 N, after which an increment of the applied displacement (0.2 mm) corresponds to a small decrement of the external load, and this corresponds to the full development of the bridging area. This will be discussed in Section 4.3. Secondly, a discrepancy between the experimental and numerical results was found in the first FE run (dashed line). A close examination of the failed fracture surface revealed that the position of the first z-pin row was misplaced just at 1 mm ahead of the initial crack position instead of the usual distance of 5 mm (Fig. 4a), for which the FE model mimicked initially. The FE model for this case was then adjusted by placing the interface z-fibre elements at the experimentally measured position. The effect of z-pining on the elastic constants of the laminate was also taken into account by considering a more compliant laminate in the z-pinned area of the laminate. This was done by changing the stiffness matrix constants of the elements in the z-reinforced region of the model [13]. The revised FE model showed a much better agreement with the experimental data. This example demonstrates also the capability of the FE model developed in this study.

4.3 Large scale bridging effect

The LEFM theory assumes that all energy dissipations are confined within the crack tip zone. However, for reinforced laminates the z-fibres within the bridging zone will actively bridge the crack wake by producing traction forces and consuming large amount of energy, which will delay the delamination progress. Our FE analysis has found that the bridging force function $\Phi_z(x)$ will reach its maximum value Φ_{max} within the LSB zone that has length D and width B. It is also found that the maximum bridging effect is related to the numbers of active z-fibre rows, the maximum bending moment, laminate stresses, and the maximum bridging length. These findings are summarised below and illustrated in Figs. 8-9.

A steady LSB zone would be developed soon after the first z-pin row was pulled out. During the subsequent crack growth the LSB zone moved forward along with delamination front. Behind the LSB zone there was no traction force because those z-pins had already been pulled out (ψ_z=0, Fig. 8). Similar steady-state processes were reported for DCB specimens of the conventional laminates [17] and in stitched laminates when the bridging entities started failing [11]. When the LSB process is fully developed, the bridging function $\Phi_z(x)$ reached a constant value. In terms of the bridging force offered by each individual pin, ψ_z, when a new row of z-pins enters in the bridging zone another row will fail (z-pins pullout) leaving the total amount of bridging forces acting in the bridging area almost constant. Then essentially we can write:

$$\Phi_Z \cong const \quad \& \quad \sum_1^n \psi_i \cong const \tag{11}$$

The scenario expressed by Eq. 11 can be further demonstrated by Fig. 9 that shows the number of z-pin rows (left axis) versus delamination growth length. The white columns refer to the total number of z-fibre rows involved in the bridging process, the grey bars represent number of z-fibre rows in the maximum bridging area, and the black bars represent the z-pin rows that have already been pulled out (ψ_z=0). The open-circle points correspond to the number of z-fibre rows where the maximum bending moment occurred. The smooth curve plots the ratio of number of z-fibre rows in the Φ_{max} area to the total number of working z-pin rows; the value refers to the y-axis on the right hand side.

4.4 Effect of z-fibre density

Computational *P-δ* curves for both z-pinned (four volume densities of 0.5%, 1%, 2%, and 4% with z-fibre diameter of 0.28 mm) and un-reinforced DCB specimens are presented in Fig. 10. Firstly, these *P-δ* curves showed that the work done for the onset of delamination extension (at *P≅40N*) did not change between the pinned and unpinned models, while during the crack growth stage the work done for the reinforced specimens rose to the values that were one order of magnitude higher than the that of the unpinned case. Secondly as soon as the delamination came across the z-pin bridging field the curve slope changed, which was a function of the z-pin density.

The maximum load in the *P-δ* curves is related to the pullout of the first z-fibre row defining the starting point of the second stage of the delamination process when the so-called LSB is fully developed. It is also noted that the displacement value at which the maximum load occurred increased with the increasing z-pin density.

However, the comparison of z-pin density effect in terms of *P-δ* relationship as made in Fig. 10 lacks the necessary information about the growing delamination lengths and delamination front positions. Therefore, the external load (*P*) is also plotted against the delamination length (*a*) in Fig. 11, which shows computational results (points) and polynomial fitted curves. The un-pinned specimen showed a decreasing external load (*P*) against the propagating delamination, i.e. less force was required as the crack became longer. However, for all reinforced laminates the external load had to increase in order to advance the crack until the load reached its maximum value after which a slowly decreasing external load against crack length was predicted. In terms of structural design the above result is significant. For example, in order to propagate a crack to 15 mm, a load of 37N would be sufficient for an un-reinforced laminate, whilst the z-fibre reinforced laminate needed much higher external load, e.g. 65, 98, 158, and 240 N, respectively, for the various z-pin densities investigated. On the other hand, if the design load is defined, upper and lower bounds of the required z-fibre density can be determined.

The rising part in the *P-a* curves is characteristic of z-pinned laminate. This represents the stage when the first few z-pin rows are engaged in the bridging process. The stable LSB process will follow when *P* reached its summit. Note the sharp rise in the higher z-pin density cases. Those models that use uniformly distributed z-pin traction forces would have difficulties to capture the sharp rise of the external force.

For a higher z-pin density, the number of z-fibre rows involved in the bridging zone is also larger. Therefore, the displacement of the DCB arms would be larger in the LSB zone as shown in Fig 10, and this will force the first row of z-fibres to stretch, debond, and pullout more quickly comparing to the cases of lower density reinforcement. Therefore, the higher the z-fibre density, the shorter the crack length at the summit of the *P-δ* curves (Fig. 11) and the higher the non-linearity of structural deformation would be.

From the finite element results the number of times when delamination is temporally arrested can be worked out by counting the consecutive load points where the load is increasing but the delamination length is constant (Fig. 11). It is found that the crack length at temporary arrestment corresponds to the involvement of a new z-fibre row entering the bridging process; as soon as the delamination front comes across a new z-fibre row and the displacement vector *u* of the new bridging row becomes greater than zero ($\psi_z=F(u)>0$), the crack will be arrested temporally. This phenomenon is more visible in laminates with low-density z-pins than those with high-density pins in which cases crack arrestment can occur more often due to more pins bridging the crack. For example, after 15 mm crack growth the 0.5% density pinned laminate had 3 rows of z-pin involved in the bridging process, 1% had 4 activated rows, 2% had 6 rows bridging the crack, and 4% had 7 working rows (Fig. 11).

4.5 Effect of z-fibre diameter

Fig. 12 shows the results of external load (P) against delamination length (a) for two z-fibre radii (r_1=0.14 mm and r_2=0.25 mm). The z-fibre density was kept constant (2%) in the FE models by placing the interface elements at different positions as indicated in Table 1. All the other parameters of the finite element and micro-mechanical models were unchanged. The result of unpinned specimen is also reported for comparison. The better performance of the smaller z-fibre radius (r_1) was demonstrated. When the LSB process was fully developed, the laminate pinned by smaller diameter z-fibres provided more resistance to delamination growth; the external load was almost doubled than that by using the thicker z-fibre (r_2) option. The FE results also shows that before reaching the stable bridging configuration at the same crack length of 16 mm seven rows of thinner z-fibres (radius r_1) and four rows of thicker z-fibres (radius r_2) were passed by the delamination front, respectively.

Since most energy dissipation is spent during the z-pin pullout process, smaller z-fibre diameter will be a better choice. This was also confirmed by the micro-mechanics solutions [5, 27].

4.6 Effect of friction energy

The interfacial frictional stress (τ) between a z-fibre and the surrounding laminate during frictional sliding will also affect the value of z-fibre bridging traction force. In [19,23] typical range of the frictional stress was suggested to be between 10 and 80 MPa for the same range of z-fibres and laminate systems used for this study. Fig. 13 shows the effect of different frictional stresses ($10 \leq \tau_i \leq 25$ MPa) on delamination growth in terms of external load (P) against propagating delamination length (a) for the case of 0.5% density pinned laminate with 0.28 mm diameter carbon pins. An increased friction shear stress (τ) corresponds to an increased LSB effect. When τ increases, the maximum load position shifts to the left of the graph indicating a smaller bridging domain (D) but more resistant to further delamination. Therefore, the higher the frictional energy dissipated, the lower the number of z-pin rows actively involved in the bridging process, and the smaller the crack length when stable constant bridging process occurs. Comparing the plots in Figs. 11 and 13 it is noticed that the 0.5% density pinned laminate with an assigned friction stress of 25 MPa could generate a LSB zone that is equivalent to the one of a 1% density reinforced laminate with a friction shear stress of 15 MPa. Therefore from a design point of view, if higher frictional resistance can be achieved, then lower density z-pinning could be applied introducing less in-plane fibre waviness and less stiffness degradation, saving weight and costs in reinforcing the structure.

To achieve higher frictional shear stresses and therefore higher bridging forces different options are available: enhancing the z-fibre surface roughness, choosing appropriate resin system, and optimising the radial stresses arising from the initial thermal mismatch between the z-fibres and surrounding materials.

4.7 Effect of laminate flexural rigidity and z-fibre insertion depth.

Fig. 14 shows the effect of the laminate elastic modulus on delamination growth of z-pinned laminates. The slopes of the curves either before or after the fully developed LSB process were almost the same for the three selected laminates with different elastic moduli (E_x). Only the values for the initial delamination load, the maximum load, and relative crack position were moderately affected by the difference in laminate elastic properties. From the value of the crack length where LSB process attained a steady-state, it can be concluded that the more compliant the laminate arms, the fewer z-pin rows involved in the LSB process and the smaller the crack length for stable bridging will be.

According to a previous study the Young's moduli of pinned laminates are about 7-10% lower than those of unpinned laminates [13]. Hence correct moduli for pinned laminates were used in the numerical simulations. However, the numerical results showed that the laminate Young's modulus does not affect the z-fibre displacement vector (u) and thus indirectly, its bridging behaviour noticeably; the bridging load (ψ_z) is governed by the micromechanical parameters of the z-fibre (Eq. 4). In this case the rigid pullout of a z-

fibre is the dominant mechanics that is governed by the friction stress (τ) between the z-fibre and the laminate.

Fig. 15 shows the effects of thickness (*2t*) of the DCB and z-fibre insertion depth (*d*) along with the results for the unpinned specimens. Firstly, the thickness variation affects laminate flexural rigidity and therefore as the previous computation (Fig.14) a small translation of the maximum load position to a longer delamination length. For the 3 mm thick (*2t*) laminate after 15 mm of delamination propagation the LSB is fully developed, but for the thicker laminate (*2t=6*) with the maximum z-pin embedding depth (*2t=2d=6 mm*), 30 mm crack is needed for all z-fibres actively bridging the crack wake. In terms of the z-fibre insertion depth (*d*), for the same z-pin density and diameter, the deeper the z-fibre embedded in the laminate, the higher the required load would be to propagate the delamination. As for the case of the frictional stress, when the dominant mechanism is the z-pin pull-out process a more resistant LSB function can be achieved by a deeper embedding depth (*d*); the best embedding depth is the full laminate thickness.

4.8 Energy balance and fracture toughness during LSB

As a by-product, the energy balance described by Eq. (5) was calculated from the FE outputs. In Fig. 16 individual energy components of the DCB are plotted against the delamination length. The graph refers to a DCB model reinforced by z-fibres of 1% density and 0.28 mm pin diameter. When the delamination propagated into the first 5 mm (no z-pins in this region), the difference between the total external work (*W*) and the elastic deformation energy (U_e) equalled to the fracture energy at the delamination front (Γ). The LEFM assumption remains valid until the crack reaches 11 mm. From this stage the energy absorbed by the LSB mechanism (U_{ir}) became higher than the energy dissipated at the delamination front. The term U_{ir} could not be neglected anymore. Moreover, since U_{ir} increased significantly with the delamination growth, the difference between the external work (*W*) and the stored deformation energy (U_e) had to increase in order to provide more driving force for crack growth. Since the fracture energy at delamination front (Γ) depends only on the properties of the laminate, the Γ curve should be a constant for any pin diameters. Based on these findings, a good design approach for z-fibre reinforced structures should aim at maximizing the energy absorption capability (U_{ir}) during the LSB process.

The energy rates per unit crack extension, G_I, Φ_{ir}, and G_{IC}, as defined by Eq. (8), were also calculated and shown in Fig. 17. At a very small cohesive zone of the crack tip, the fracture surface energy rate G_{IC} has a constant value of 250 J/m^2 for both pinned and unpinned laminates. The "square" and "star" symbols represent the computational results of strain energy release rate (G_I) and energy dissipation rare (Φ_{ir}), respectively. The smooth lines are fitted curves. The results confirm the energy rate balance for z-pinned laminates described by Eq. (9). The strain energy release rate (G_I) defined in Eq. (8) represents the toughness of a z-pinned laminate during mode I crack growth. Therefore, it is possible to validate the G_I values by experimentally measured data, and then to quantify the calculated Φ_{ir} values indirectly given that G_{IC} is a constant of the material.

5. Conclusions

A numerical approach that combines the computational accuracy and versatility of the finite element method with an existing micro-mechanical material model is presented. The numerical simulation was executed by including as many parameters as possible to characterise the mode I fracture behaviour of z-pinned laminate. Satisfactory agreement with experimental data was obtained. Following conclusions may be drawn.

The z-fibre technique is very effective in enhancing the resistance to mode I delamination growth. The relationship of external load versus delamination length is found to be a better indicator for the fracture resistance and the large scale bridging effect. However, z-pinning had no noticeable effect on the onset (or

initiation) of delamination growth from a starter crack. This observation is consistent with the experimental results.

The effectiveness of z-pinning is mainly owing to the formation of a large scale bridging (LSB) zone behind the advancing crack. The LSB can become a stable process when some z-fibre rows are pulled out from the laminate. In order to activate the z-fibre bridging mechanism a delamination crack needs to propagate into the z-fibre field for several millimetres; the LSB can then stabilize or even temporally arrests the delamination crack. Therefore z-pinning is very useful for damage tolerance design. The magnitude of the LSB is independent of the crack length; an almost constant bridging area translates forward as the crack propagates.

Delamination resistance can be further enhanced by choosing higher z-fibre density, increasing friction stress at the laminate and z-pin interface, employing finer z-fibre diameters and deeper z-fibre embedding depth. The laminate flexural rigidity influences the number of working z-pin rows in the LSB zone and the crack length at which the LSB process will reach a steady state.

In terms of energy balance z-pinned laminates have good capability of energy absorption. During delamination growth the large scale bridging process absorbs considerable amount of energy that otherwise would have been used for delamination growth. The assumption made by the LEFM that all energy dissipations are included in the fracture energy and confined within the damage front is not valid for z-pinned laminates. The irreversible energy dissipation due to z-pins pulling out becomes the dominant term in the energy balance to enhance the fracture toughness of z-fibre reinforced laminates.

Acknowledgements

References

1. Freitas G, Fusco T, Campbell T, Harris J, Rosenberg S. Z-Fiber[TM] technology and products for enhancing composite design. *83rd Meeting of AGARD Structures & Materials Panel*. 1996.
2. Freitas G, Fusco T, Magee C, Dardzinski P. Z-Fibre insertion process for improved damage tolerance in aircraft structures. *J of Advanced Materials 1994;* 25.
3. Dow MB, Smith DL. Improving the delamination resistance of CFRP by stitching carbon fabrics. *21st Int. SAMPE Technical Conference* 1989, 595-605.
4. Partridge IK, Cartié DDR, Bonnington T. Manufacture and performance of Z-pinned composites. Chapter 3 in Advanced Polymeric Materials: Structure Property Relationships, eds S Advani and G Shonaike, CRC Press LLC, April 2003.
5. Rugg C, Cox BN, Ward KE, Sherrick GO. Damage mechanics for angled through-thickness rod reinforcement in carbon-epoxy laminates. *Composites Part A* 1998; 29A: 1603-1613.
6. Rugg KL, Cox BN. Mixed mode delamination of polymer composite laminates reinforced through the thickness by z-fibers. *Composites Part A* 2002; 33: 177-190.
7. Troulis M, Cartié DDR, Partridge IK. Z-Pinned woven laminates: interlaminar fracture results and pinning quality considerations. Proc of Sixth Int Conf on Deformation and Fracture of Composites (DFC6), Manchester, 2001.
8. Cartié DDR, Partridge IK. Delamination behaviour of Z-pinned laminates. In Proc 2nd ESIS TC4 Conference. Eds JG Williams and A Pavan, Elsevier, 2000, ESIS Publication 27 "Fracture of Polymers, Composites and Adhesives". ISBN/0080437109.
9. Tanzawa Y, Watanabe N, Ishikawa T. Interlaminar fracture toughness of 3-D orthogonal interlocked fabric composites. *Comp Sci & Tech,* 2001; 61:1097-1107.
10. Dransfield K, Baillie C, Mai YM. Improving the delamination resistance of CFRP by stitching - a review. *Comp Sci Tech;* 1994; 50: 305-317.

11. Dransfield AK, Jain LK, Mai YW. On the effect of the stitching in CFRP- I. Mode I delamination toughness. *Comp Sci Tech* 1998; 58: 815-827.

12. Tong L, Jain LK, Leong KH. Failure of a transversely stitched RTM lap joint. *Comp Sci Tech 1998:* (58): 221-227.

13. Grassi M, Zhang X, Meo M. Numerical prediction of stiffness and stresses in z-fibre reinforced laminates. *Composites Part A: Applied Science & Manufacturing*, 2002; 33: 1653-64.

14. Craig A, Fleck NA. Z-pinned composite laminates: knockdown in compressive strength. *Fifth Int Conf on Deformation and Fracture of Composites (DFC5), London*. 1999. pp. 60-68.

15. Dickinson LC, Farley GL, Hinders MK. Prediction of effective three-dimensional elastic constants of translaminar reinforced composites. *J of Comp Materials* 1999; 33: 1002-29.

16. Bao G, Suo Z. Remarks on crack bridging concepts. *Applied Mechanics Review* 1992; 45: 355-366.

17. Sorensen BF, Jacobsen TK. Large-scale bridging in composites: R-curves and bridging laws. *Composites Part A* 1998; 29A: 1443-1451.

18. Lindhagen JE, Berglund LA. Application of bridging-law concepts to short-fibre composites. Part 1: DCB test procedures for bridging law and fracture energy. *Comp Sci Tech* 2000; 60: 871-883.

19. Liu HY, Mai HW. Effects of z-pin reinforcement on interlaminar mode I delamination. Proc of 13th Int Conf on Comp Materials (ICCM-13), Beijing, July 2001.

20. Mabson GE, Deobald LR. Design curves for 3D reinforced composite laminated double cantilever beams. *Proc of ASME Int. Mechanical Eng. Congress and Expo.* 2000, pp 89-99.

21. Massabo R, Cox BN. Unusual characteristics of mixed mode delamination fracture in the presence of large scale bridging. *Mechanics of Composite Materials and Structures* 2001;8: 61-80.

22. Barrett DJ. The mechanics of z-fibre reinforcement. *Composite Structures* 1996; 36: 23-32.

23. Cartié DDR. Effect of z-fibres on delamination behaviour of carbon-fibre/epoxy laminates. PhD Thesis, Cranfield University, U.K.

24. Cox BN, Massabo R, Rugg K. The science and engineering of delamination suppression. *Sixth Int Conference on Deformation and Fracture of Composites* (DFC6), Manchster, 2001. 3-12.

25. Zhang X, Liu HY, Mai YW, Diao XX. On steady-state fibre pull-out – I. the stress field. *Comp Sci Tech* 1999; 59: 2179-2189.

26. Zhang X, Liu HY, Mai YW, Diao XX. On steady-state fibre pull-out – II. computer simulation. *Comp Sci Tech* 1999; 59: 2191-2199.

27. B. N. Cox and N. Sridhar. A Traction law for inclined fibre tows bridging mixed mode cracks. <u>Mechanics of Composite Materials and Structures</u>, **9**, 299-331 (2002).

28. Cox BN. Constitutive model for a fiber tow bridging a delamination crack. *Mechanics of Composite Materials & Structures* 1999; 6:117-138.

29. Crisfield MA. Non-linear finite element analysis of solids and structures. 1997.

30. Mi Y, Crisfield MA, Davies GAO, Hellweg HB. Progressive delamination using interface elements. *Journal of Composite Materials* 1998; 32: 1247-1272.

31. Shen F, Lee KH, Tay TE. Modelling delamination growth in laminated composites. *Comp Sci Tech* 2001; 61: 1239-1251.

32. Borg R, Nilsson L, Simonsson K. Simulation of delamination in fibre composites with a discrete cohesive failure model. *Comp Sci Tech* 2001; 61: 667-677.

33. ANSYS Structural and Analysis Guide. SAS IP Inc. Chapter 8: Non-linear structural analysis. 2001.

34. Rybicki EF, Kanninen MF. A finite element calculation of stress intensity factors by a modified crack closure integral. *Eng Fract Mech* 1977; 9: 931-938.

35. Glaessgen EH, Riddell WT, Raju IS. Effect of shear deformation and continuity on delamination strain energy release rates. 39th AIAA/ASME/ASCE/AHS Structures, Structural Dynamic and Materials Conference. 1998; AIAA Paper 98-2002.

36. Wang JT, Raju IS. Stain energy release rate formulae for skin-stiffener debond modelled with plate elements. *Eng Fract Mech* 1996; 54: 211-228.

37. Raju IS, Sistla R, Krishnamurthy T. Fracture mechanics analyses for skin-stiffener debonding. *Eng Fract Mech* 1996; 54: 371-385.

38. O'Brien TK. A shell/3D modelling technique for the analysis of delaminated composite laminates. *Composites Part A* 2001; 31: 25-44.

39. Jones R, Alesi H. On the analysis of composite structures with material and geometric non-linearities. *Composite Structures* 2000; 50: 417-431.

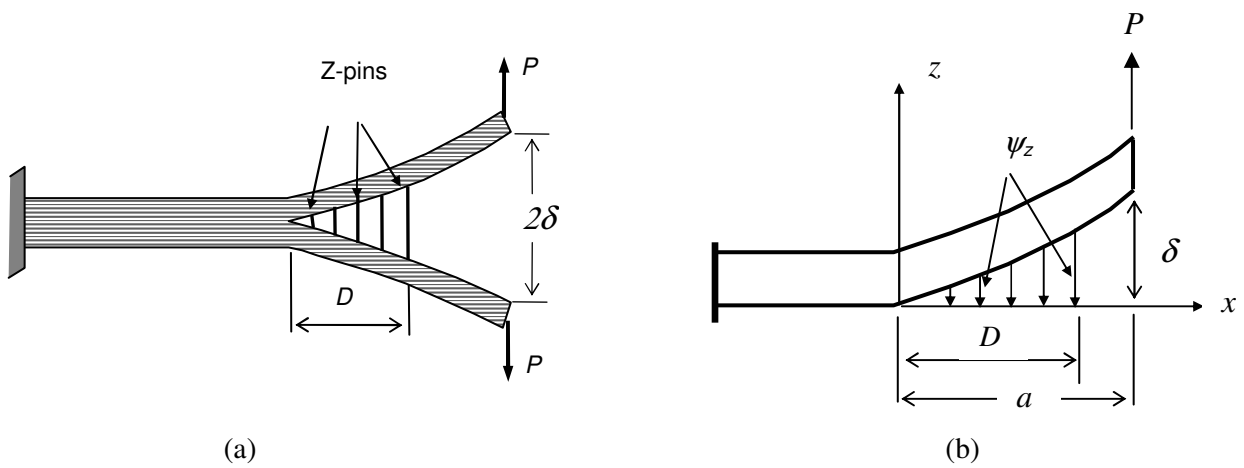40. Gdoutos EE, Pilakoutas K, Rodopoulos CA. Failure Analysis of Industrial Composite Materials. McGraw Hill, 2000.

Fig. 1 (a) Schematic of a Double Cantilever Beam (DCB) test for z-pinned laminate; (b) Beam model for a DCB arm with discrete z-fibre bridging forces, $\psi_z(x)$, acting over the length of the large-scale bridging zone (D).
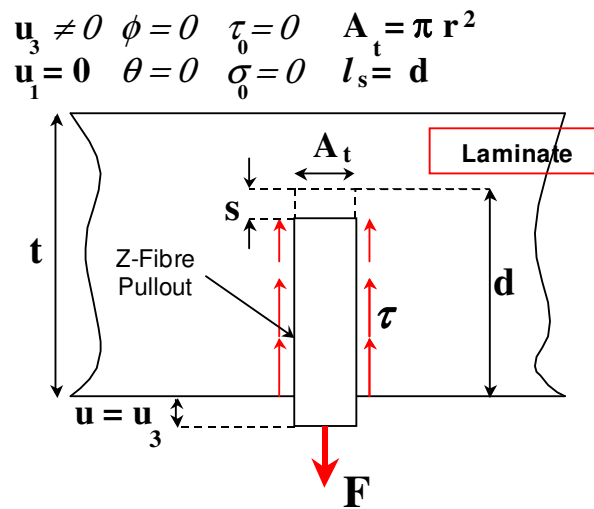
Fig. 2 Micro-mechanical model for a single z-fibre under mode I loading and boundary conditions.
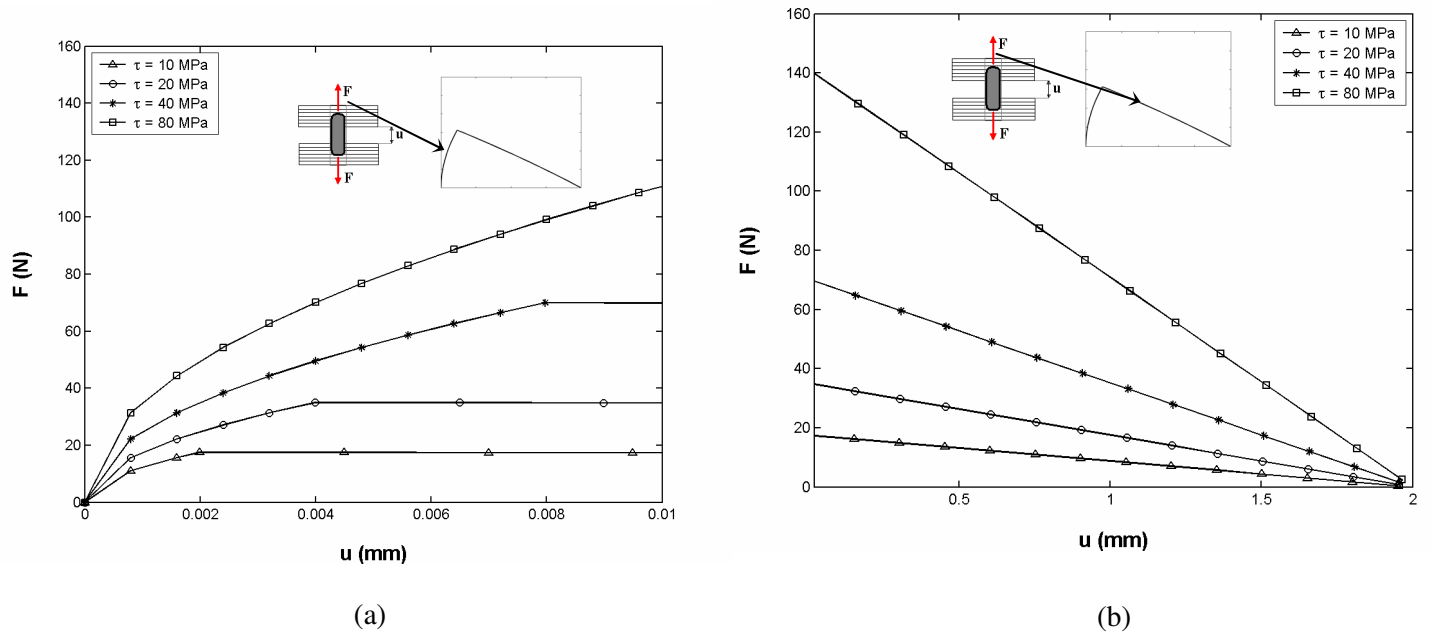
Fig. 3 Computed load-displacement (*F–u*) curves for single z-fibre pullout with influence of different friction stresses: (a) stable slip stage; (b) stable frictional sliding stage. Notice the scales of x-axis.
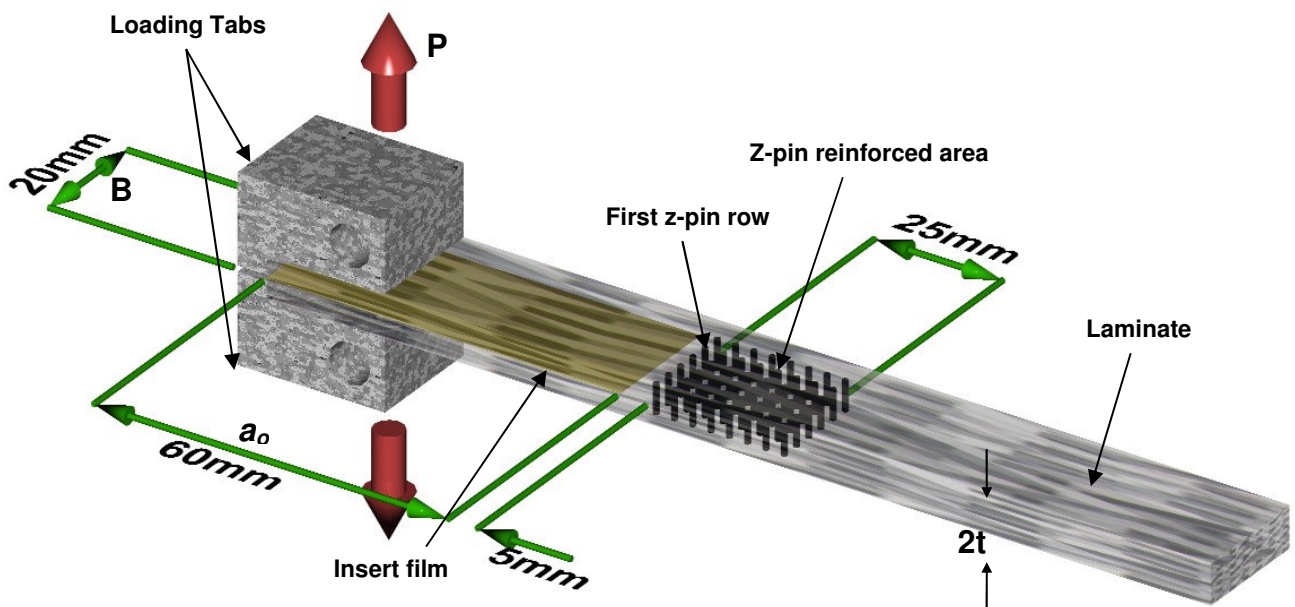
Fig. 4 (a) Z-fibre reinforced DCB specimen used in this study. Notice the distance for the insert film to the first z-pin row.
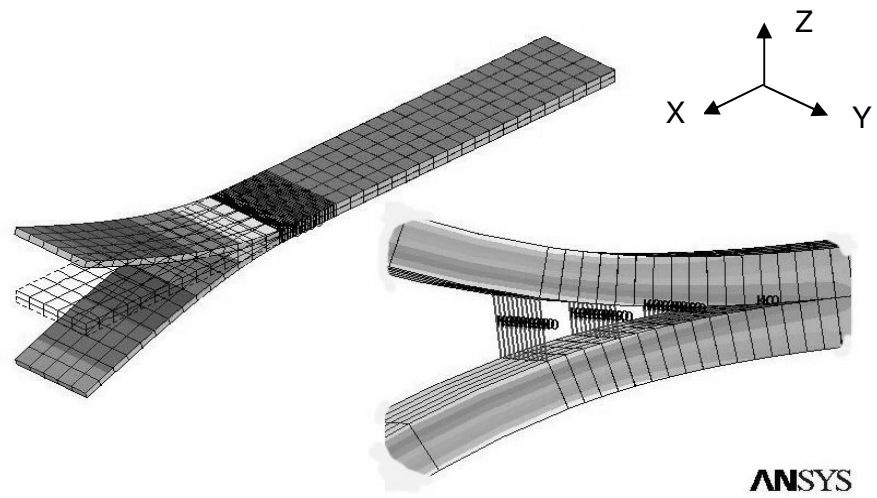
Fig.4 (b) FE model of the DCB specimen.
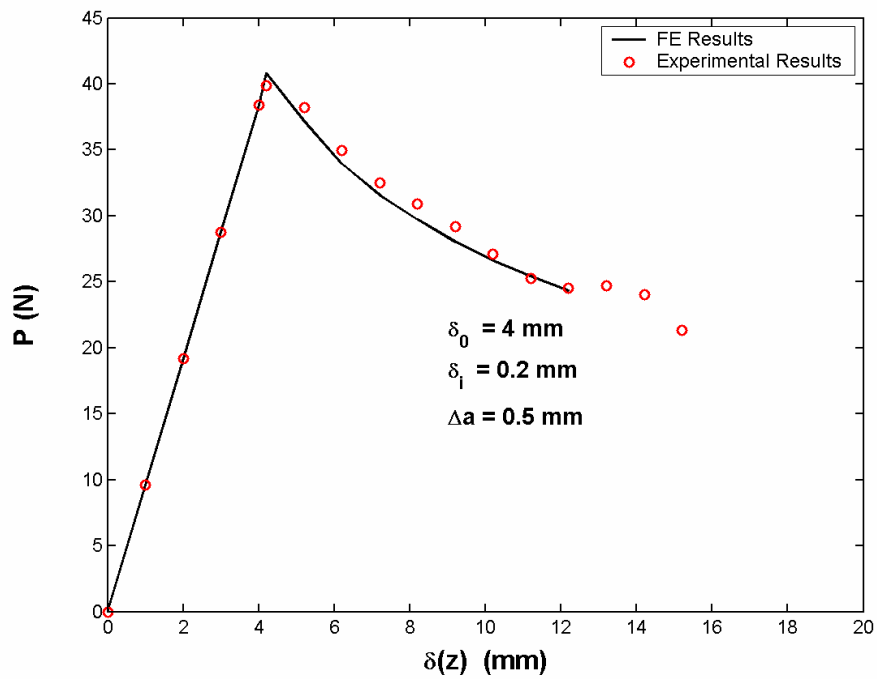
Fig. 5 Load-displacement relation for unpinned DCB (control case) – numerical vs. experimental results.
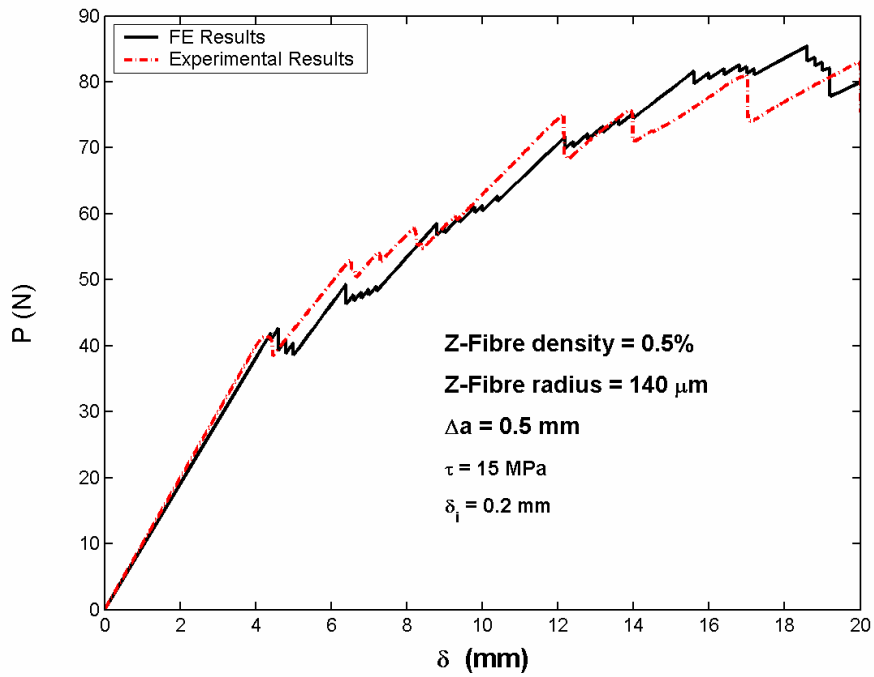
Fig. 6 Load-displacement curves for z-pinned DCB – Numerical vs. experimental results.
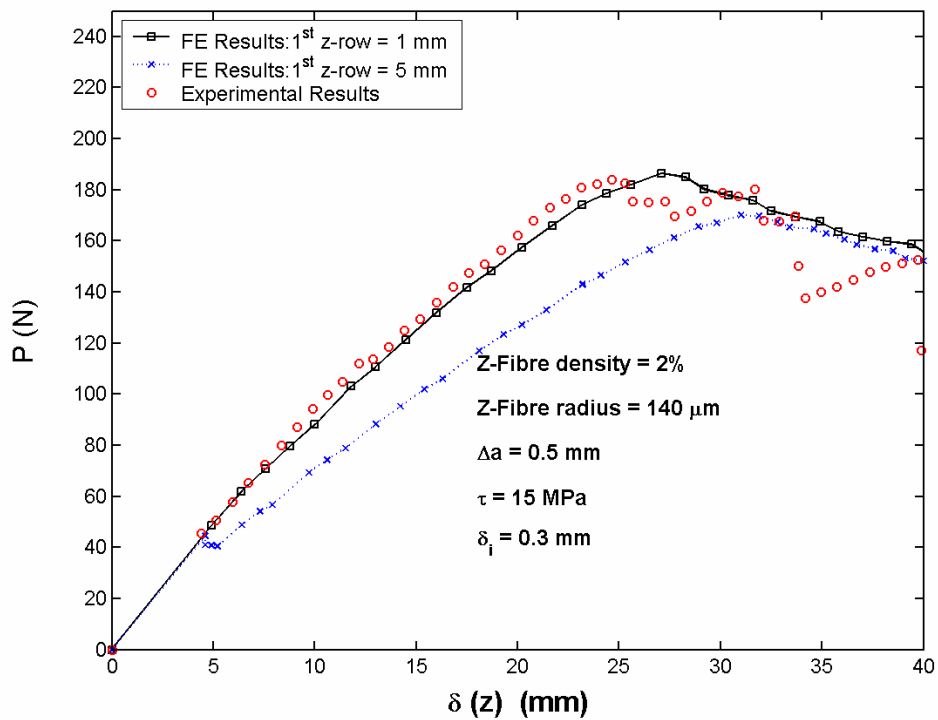
Fig. 7 P-δ curves for a 2% z-pinned DCB. Note: experimental specimen: first z-pin row was misplaced at 1 mm from the crack tip; two FE models: distances between the first z-pin row to the crack tip were 5 mm and 1 mm (same as the experiment), respectively.
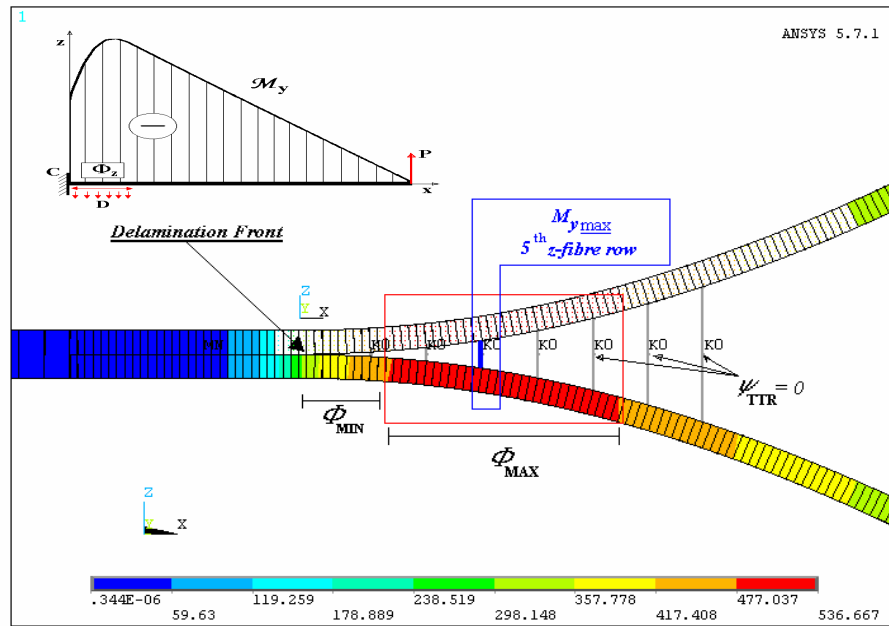
Fig. 8 The Φ_{max} and Φ_{min} bridging zones characterizing the high bending moment (M_y) and high stress region of z-pin reinforced laminate.
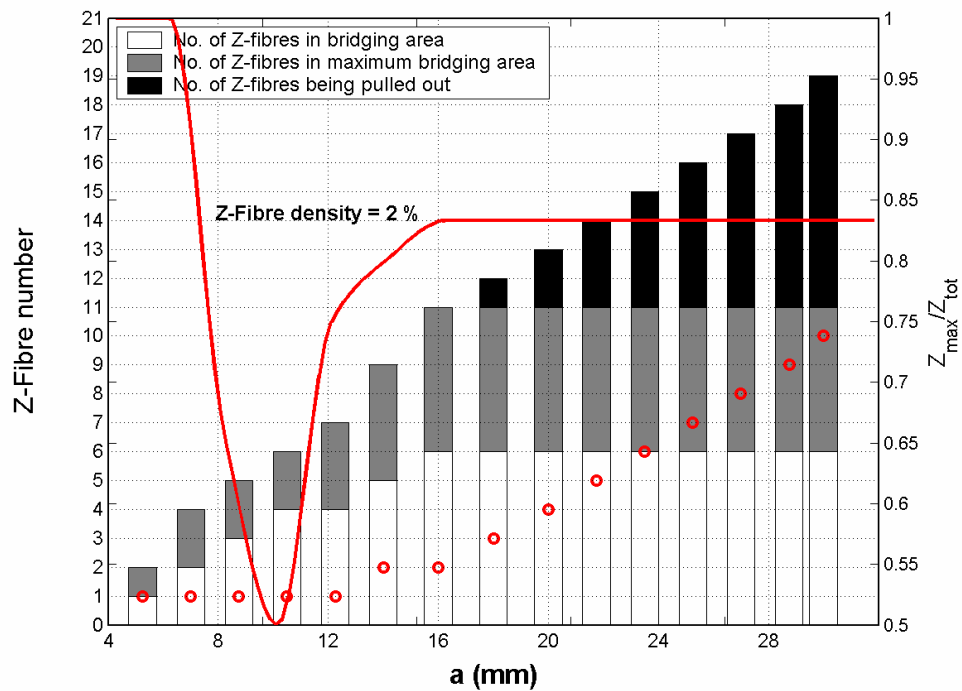
Fig. 9 Z-fibre bridging process during delamination growth for a 2% z-pinned DCB showing the numbers of z-pins involved in the different stages (bar-chart), M_{max} location (o), z-fibre ratio in Φ_{max} region (—).

19
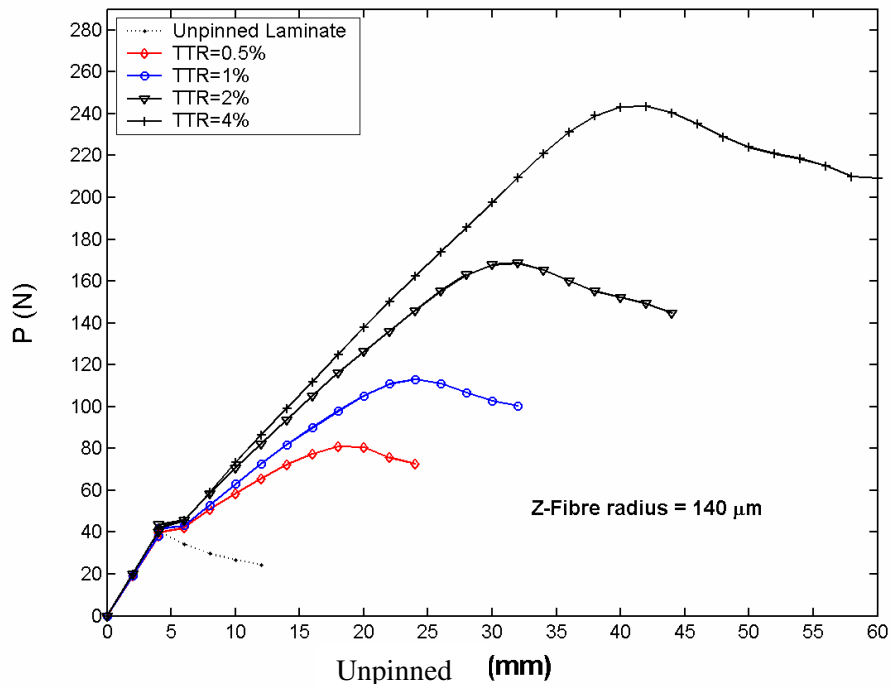
Fig. 10 Computational $P\text{-}\delta$ curves for different z-fibre densities and comparison with un-pinned case.
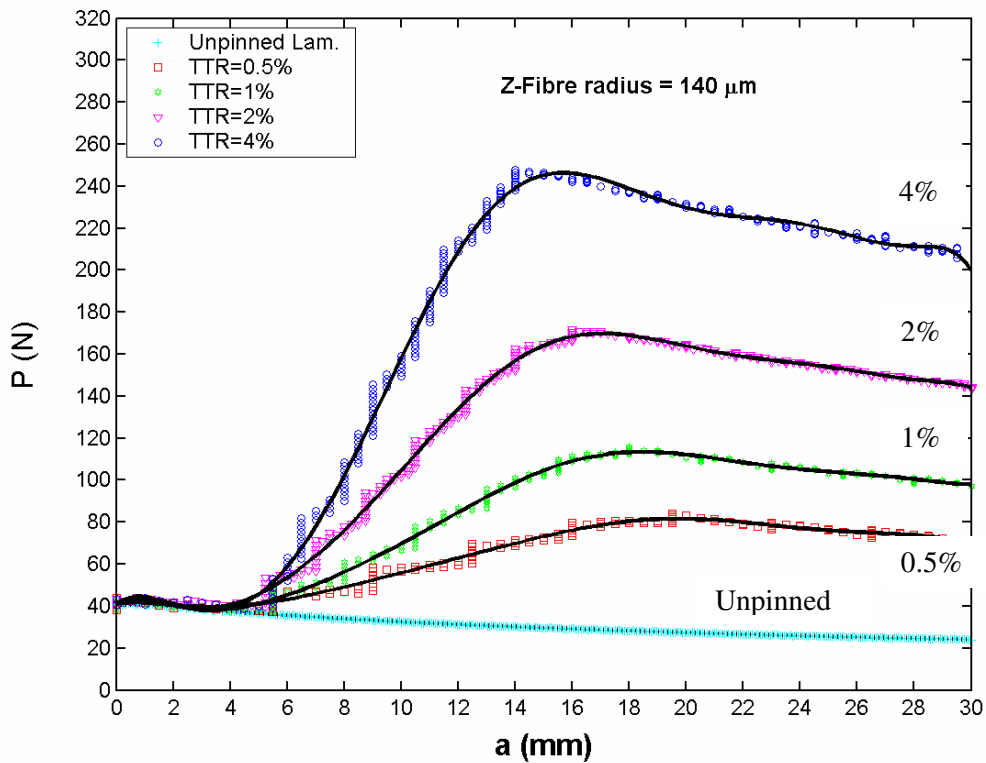
Fig. 11 Load vs. delamination length for different z-pin densities and comparison with unpinned case. FE results (discrete symbols); polynomial interpolation (smooth lines).
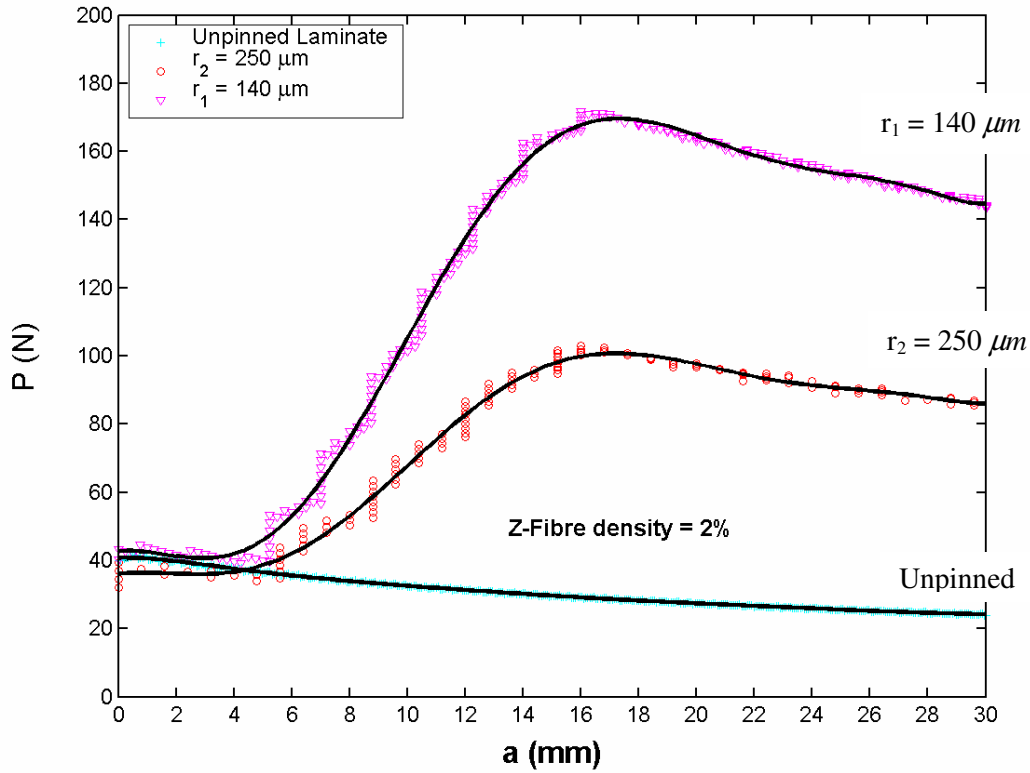
Fig. 12 Load vs. delamination length: z-pin diameter effect.
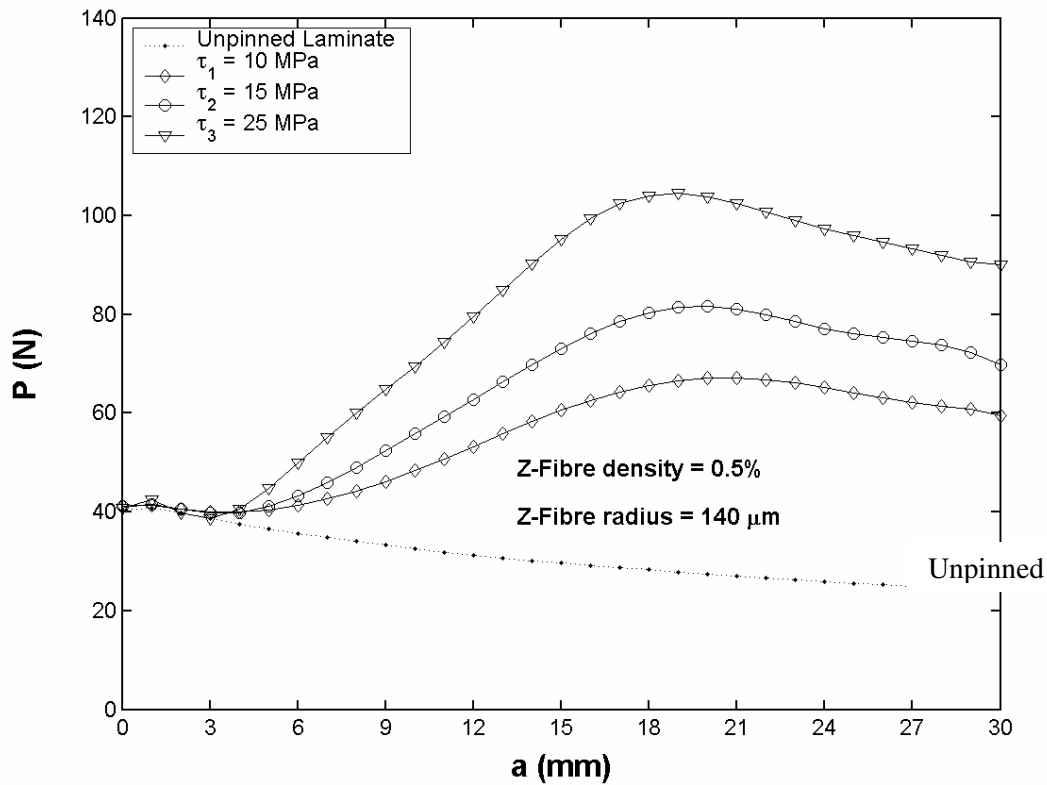
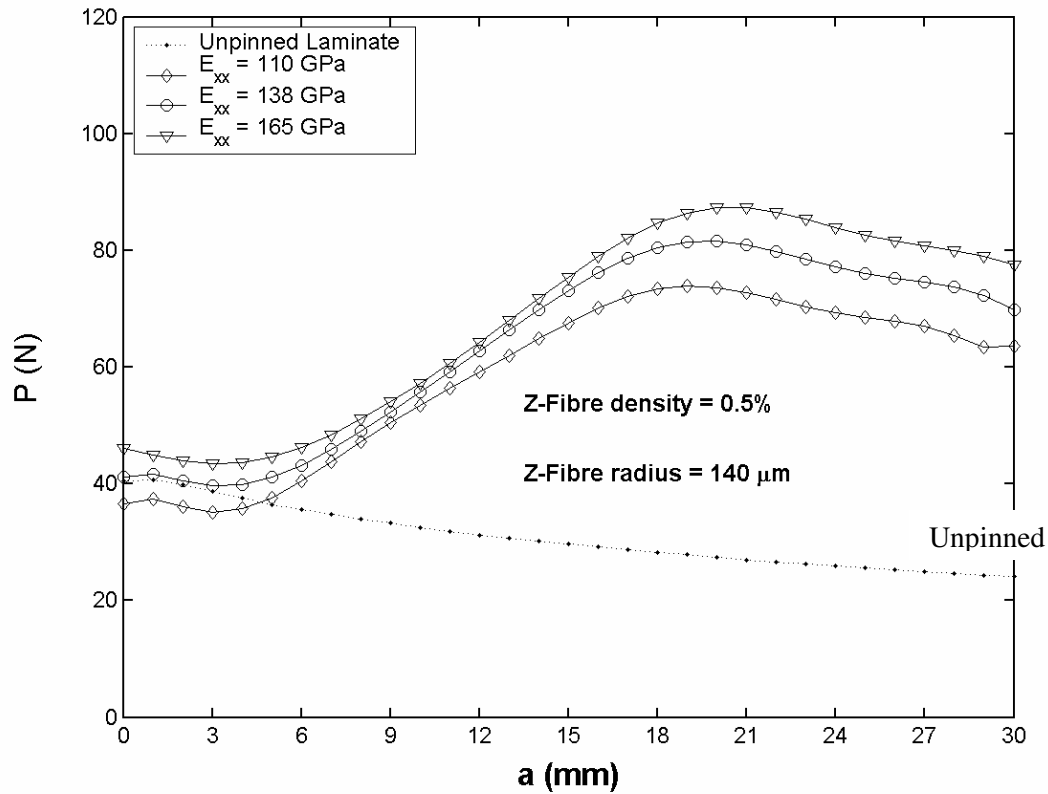Fig. 13 Load vs. delamination length: effect of frictional stress between z-fibre and laminate.

Fig. 14 Load vs. delamination length: effect of laminate flexural rigidity (0.5% z-pin density and 0.28 mm z-fibre diameter)
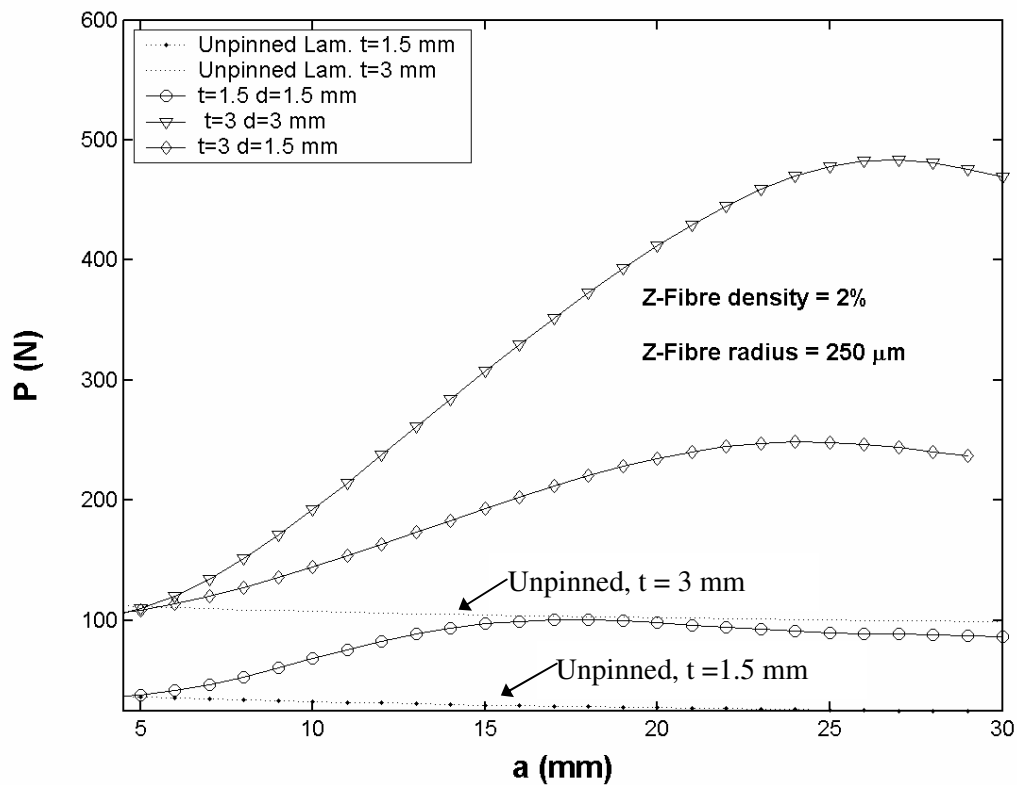

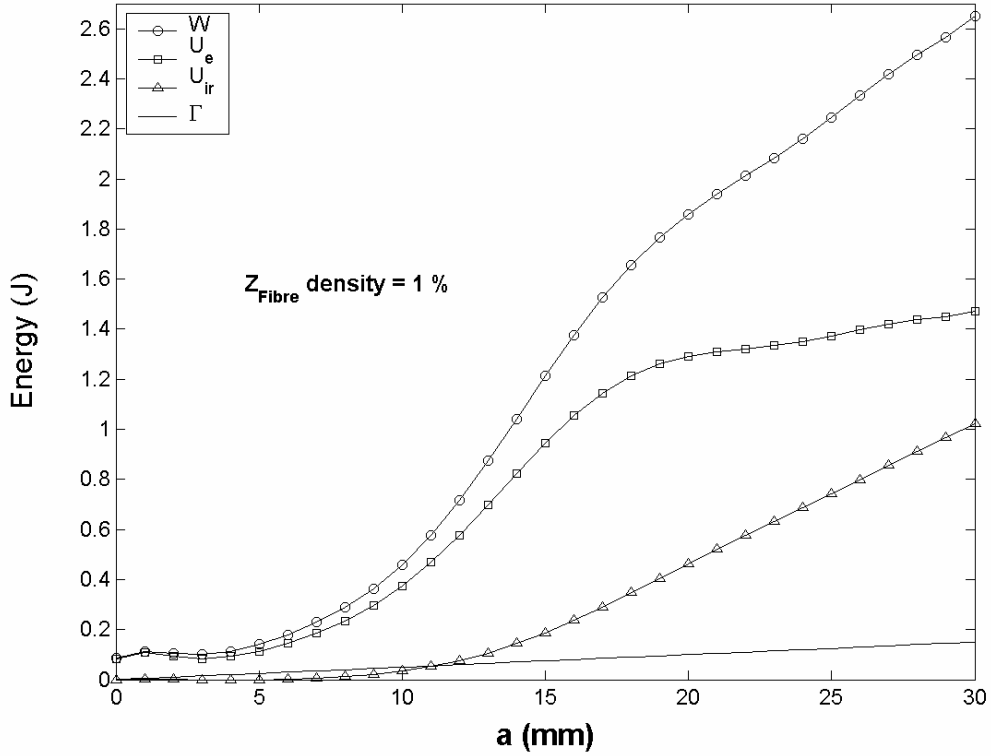Fig. 15 Load vs. delamination length: effect of laminate thickness & z-pin insertion depth.

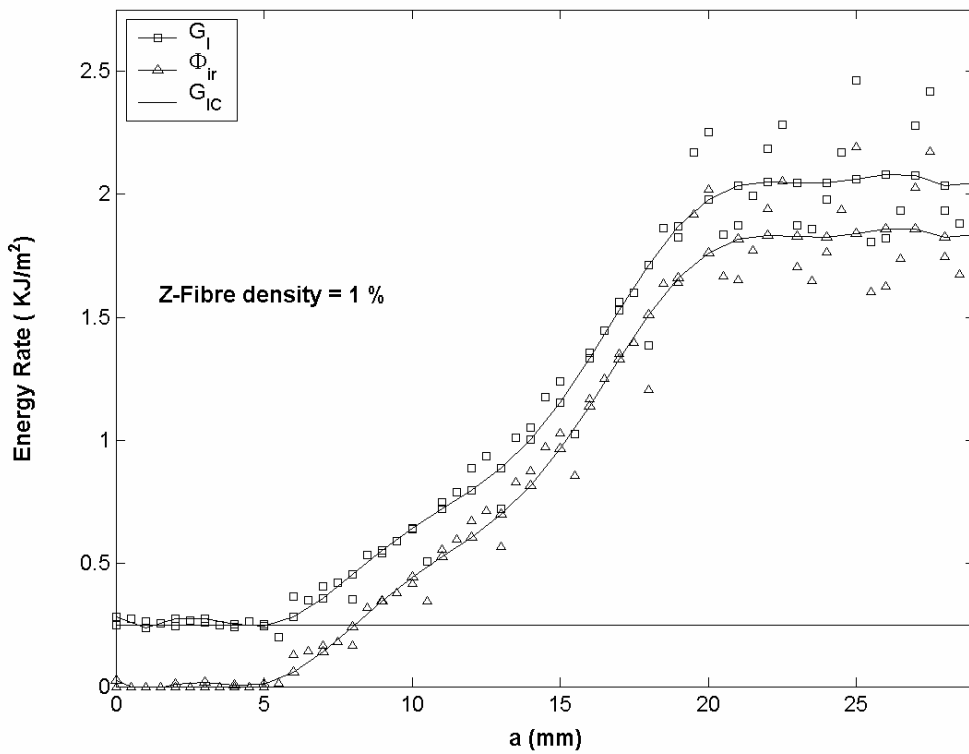Fig. 16 Energy balance during delamination and z-fibre bridging process (z-pin radius r_1).

Fig. 17 Energy rates during delamination and z-fibre bridging process (z-pin radius r_1).